1,3,4-Oxadiazole-based Deep-blue Thermally Activated Delayed Fluorescence Emitters for Organic Light Emitting Diodes

Zhaoning Li,[a,b] Wenbo Li,[c] Changmin Keum,[c] Emily Archer,[c] Baomin Zhao,[d] Alexandra M. Z. Slawin,[b] Wei Huang,[a] Malte C. Gather,*[c] Ifor D. W. Samuel*[c] and Eli Zysman-Colman*[b]*

[a] Key Laboratory of Flexible Electronics (KLOFE) and Institute of Advanced Materials (IAM), Nanjing Tech University (NanjingTech) 30 South Puzhu Road, Nanjing 211800 (China) E-mail: iamwhuang@njtech.edu.cn;

[b] Organic Semiconductor Centre, EaStCHEM School of Chemistry, University of St Andrews, St Andrews, Fife, UK, KY16 9ST, Fax: +44-1334 463808; Tel: +44-1334 463826; E-mail: eli.zysman-colman@st-andrews.ac.uk;

[c] Organic Semiconductor Centre, SUPA, School of Physics and Astronomy, University of St Andrews, North Haugh, St Andrews, Fife, KY16 9SS, UK, E-mail: mcg6@st-andrews.ac.uk; idws@st-andrews.ac.uk

[d] Key Laboratory for Organic Electronics and Information Displays & Jiangsu Key Laboratory for Biosensors, Institute of Advanced Materials (IAM), Jiangsu National Synergetic Innovation Center for Advanced Materials (SICAM), Nanjing University of Posts and Telecommunications, 9 Wenyuan Road, Nanjing 210023, China.

ABSTRACT

A series of four 1,3,4-oxadiazole-based thermally activated delayed fluorescence (TADF) derivatives are reported as emitters for organic light emitting diodes (OLEDs). As a function of the nature of the substituent on the weak 1,3,4-oxadiazole acceptor their emission color could be tuned from green-blue to blue. The highly twisted conformation between carbazoles and oxadiazoles results in effective separation of the HOMO and the LUMO resulting in a small singlet-triplet splitting. The corresponding singlet-triplet energy gaps (ΔE_{ST}) range from 0.22 to 0.28 eV resulting in an efficient reverse intersystem crossing (RISC) process and moderate to high photoluminescence quantum yields (Φ_{PL}), ranging from 35 to 70% in a DPEPO matrix. Organic light-emitting diodes (OLEDs) based on ***i*-2CzdOXD4CF$_3$Ph** achieve maximum external quantum efficiency (EQE_{max}) of up to 12.3% with a sky-blue emission at CIE of (0.18, 0.28) while the device based on ***i*-2CzdOXDMe** shows blue emission at CIE of (0.17, 0.17) with a maximum EQE of 11.8%.

KEYWORDS: oxadiazole, TADF, OLED, orientation, transition dipole, blue emitter.

INTRODUCTION

Organic light-emitting diodes (OLEDs) are now considered as one of the most promising technologies for the next-generation of large area displays and flat panel lighting because of their outstanding features; they are light, thin and can be fabricated on flexible substrates[1-7]. OLEDs based on conventional fluorescent emitters show relatively low maximum external quantum efficiencies (EQE_{max}) of 5~7.5% because only 25% of the generated excitons can be harvested

internally for fluorescence emission and in addition the out-coupling efficiency (η_{out}) is about 20%~30%[8], at least for isotropically oriented emitters. Strategies for harvesting the remaining 75% of triplet excitons have been a sustained area of research over the past two decades. Rare metal-based organometallic phosphorescent materials based on iridium(III) or platinum(II) can harvest both singlet and triplet excitons to achieve 100% internal quantum efficiency (IQE). Aside from the scarcity of these noble metals, blue phosphorescent emitters suffer from poor efficiencies and stabilities and the blue emission that is produced frequently does not meet the color coordinate requirements for high-definition displays.[9-10] Materials supporting thermally activated delayed fluorescence (TADF) possess a small singlet-triplet energy gap (ΔE_{ST}) and so can efficiently harvest triplet excitons in electroluminescent (EL) devices by reverse intersystem crossing (RISC) to the emissive singlet state.

One of the great challenges for realizing full-color displays is the development of stable and high-efficiency deep blue OLEDs. By limiting the conjugation length and selecting appropriately weak donors and acceptors, it is possible to design deep blue TADF emitters where the y-component of the color coordinate (CIE_y) is < 0.2.[11-14] Suitably weak donors are so far limited to derivatives of carbazole, diphenylamine and 9,9-dimethyl-9,10-dihydroacridine (DMAC).[15] Commonly used weak acceptors include phosphine oxides,[16-18] sulfones,[19-23] pyrimidines,[24-28] 1,3,5-triazines[29-31] and, recently, oxadiazoles.[20, 32-36] In 2012, Adachi *et al.* reported the first TADF sky-blue emitter **2CzPN**,[37] in which phthalonitrile acts as the acceptor and carbazole units act as donors. The maximum external quantum efficiency (EQE_{max}) of the OLED based on this emitter was 8.0% in this initial report. Lee *et al.*[38] reported the isomeric analog **2CzIPN** (coined in the original paper as **DCzIPN**), in which isophthalonitrile acts as the acceptor and carbazole donor

units are placed *ortho* to each of the nitrile groups. An OLED based on **2CzIPN** showed a high EQE_{max} of 16.4% and bluer CIE coordinates of (0.17, 0.19). Diphenylsulfone (DPS), with a shallow LUMO energy level of -1.37 eV, has also been exploited in the development of deep blue TADF emitters. Adachi *et al.* reported a series of pure blue TADF emitters based on a DPS acceptor and either diphenylamine, bis(4-*tert*-butylphenyl)amine or 3,6-di-*tert*-butylcarbazole donors. The respective OLEDs showed EQE_{max} of 2.9%, 5.6% and 9.9%.[39] Of these, the OLED that showed the highest EQE_{max} also was the deepest blue with CIE coordinates of (0.15, 0.07), i.e. very close to those of the National Television Standards Committee (NTSC) standard for blue defined as (0.14, 0.08). The same group reported a related emitter with DMAC as the donor, DMAC-DPS.[20] The OLED with this emitter reached EQE_{max} of 19.5% and CIE coordinates of (0.16, 0.20). We recently showed how replacement of the phenyl bridges with pyridines can result in an OLED with enhanced EQE_{max} of 13.4% and CIE coordinates of (0.15, 0.13).[40] With -1.16 eV, pyrimidine has a even shallower LUMO energy level than DPS and has therefore also been used to prepare blue TADF emitters. Yasuda *et al*.[26] developed a new platform with acridan-based donors and pyrimidine-based acceptors for high-efficiency deep-blue TADF emitters. MFAc-PPM and MXAc-PM, two of the emitters in their report, achieved a high EQE_{max} of 20.4% and 14.3% with CIE coordinates of (0.16, 0.23) and (0.16, 0.19), respectively. Kido *et al*.[24] reported a series of pyrimidine-based blue TADF emitters with EQE_{max} up to 17.8% and CIE coordinates of (0.16, 0.15).

1,3,4-oxadiazole as a building block has been widely used to construct organic or polymeric semiconductor materials because of its promising thermal stability and excellent electron injection and transporting properties.[41-44] Given its very shallow LUMO energy of -0.55 eV,[15] 1,3,4-

oxadiazole and its derivatives should be promising acceptors for deep-blue TADF emitters. However, the use of 1,3,4-oxadiazole-based acceptors within the design of TADF emitters has only been scarcely reported (Chart 1). Adachi *et al.*[32] reported 2PXZ-OXD employing 2,5-diphenyl-1,3,4-oxadiazole as the acceptor. Based in part on the choice of the strong phenoxazine donor, the OLED showed green emission with CIE coordinates of (0.25, 0.45) and EQE_{max} reached 14.9%. Huang *et al.*[45] reported the emitter BAcOX where the OLED reached an EQE_{max} of 22.3% with CIE coordinates of (0.16, 0.24) by replacing the phenoxazine donors of 2PXZ-OXD for dimethylacridan (DMAC). Marder *et al.*[34] reported a series of sky-blue TADF emitters with 2-(pentafluorophenyl)-5-phenyl-1,3,4-oxadiazole acceptors and carbazole donors. The best OLED device based on 2,3,4,5,6CzDPO reached a high EQE_{max} of 24.4% with CIE coordinates of (0.16, 0.29). More recently, Kippelen *et al.*[36] reported a host-free TADF emitter with *p*-phenylene bis-1,3,4-oxadiazole as the acceptor where the OLED showed yellow-green emission with an EQE_{max} of up to 21%. We have previously reported a series of deep-blue TADF emitters based on the **2CzPN** scaffold.[35] By replacing the cyano acceptors with functionalized 1,3,4-oxadiazole, we successfully demonstrated deep-blue to sky blue emission. An OLED based on **2CzdOXD4CF$_3$Ph** showed a maximum external quantum efficiency of 11.2% with a sky-blue emission at CIE of (0.17, 0.25), while a device with **2CzdOXD4MeOPh** showed a maximum external quantum efficiency of 6.6% with a deep-blue emission at CIE of (0.15, 0.11).

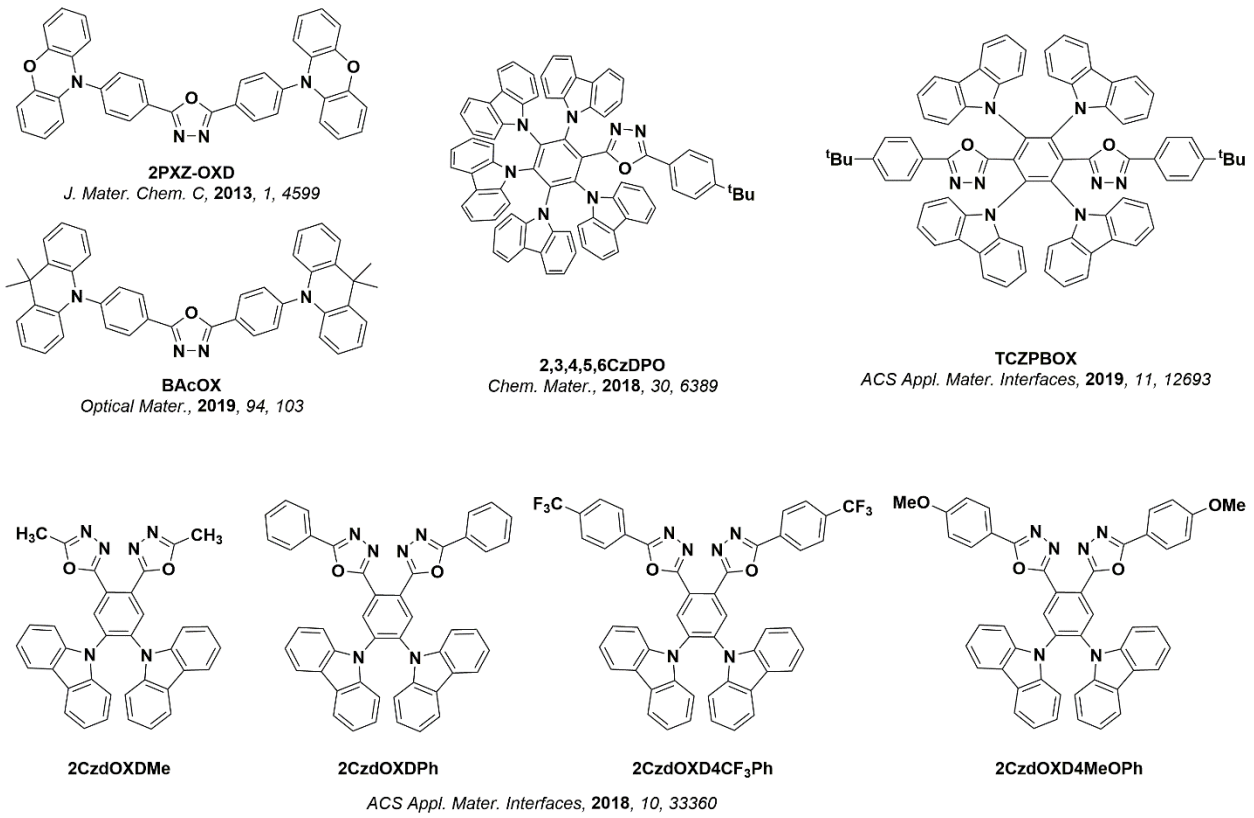

Chart **1**. Oxadiazole-based TADF emitters of previous report.

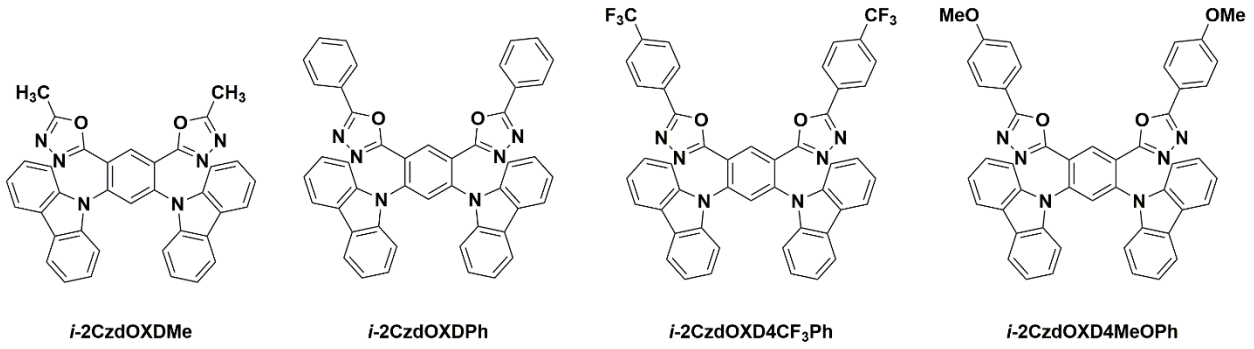

Chart **2**. New oxadiazole-based TADF emitters in this study.

In this study, we report a series of blue TADF emitters, denoted as ***i*-2CzdOXDMe**, ***i*-2CzdOXDPh**, ***i*-2CzdOXD4CF$_3$Ph** and ***i*-2CzdOXD4MeOPh** (Chart **2**). These four emitters are based on the **2CzIPN**[38] scaffold and we hypothesized that they should be even bluer emitters than

those of our initial report as the carbazole donors are disposed *ortho* to the 1,3,4-oxadiazole acceptors, which will result in increased torsion of both the donor and the acceptor leading to reduced ΔE_{ST} and higher S_1 energies. By changing the substituent groups on the 1,3,4-oxadiazole, we successfully tuned their electron-withdrawing ability and thereby influenced their emission energies. The thermal, photophysical and electrochemical properties of these compounds have been studied in detail. A comprehensive density functional theory study compliments our experiments. The dipole orientation of each TADF emitter doped into a thin-film of the host material employed in our OLEDs was investigated using angle-resolved photoluminescence (PL) spectroscopy in order to comprehensively understand the light outcoupling efficiency of our OLEDs. Finally, OLEDs based on the four TADF emitters were made and studied in detail. OLEDs based on ***i*-2CzdOXD4CF$_3$Ph** achieve an EQE_{max} of 12.3% with a sky-blue emission and CIE coordinates of (0.18, 0.28) while the device based on ***i*-2CzdOXDMe** shows deep-blue emission at CIE coordinates of (0.17, 0.17) and an EQE_{max} of 11.8%.

RESULTS AND DISCUSSION

Molecular Design and Synthesis.

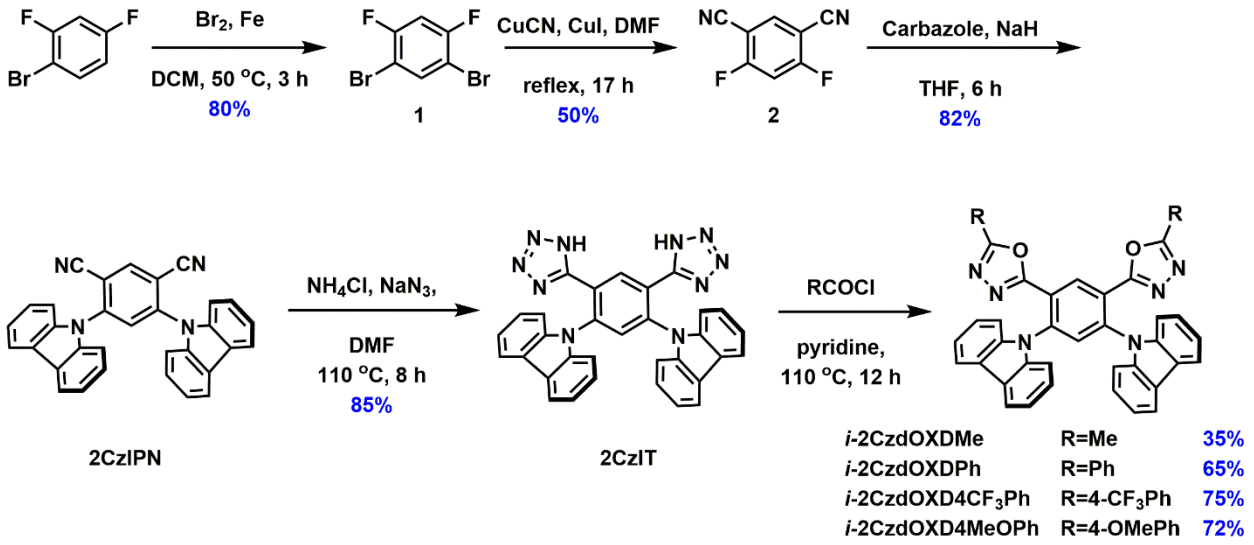

Scheme **1**. Synthesis of 1,3,4-oxadiazole-based TADF emitters.

The synthesis of the four 1,3,4-oxadiazole-based emitters is shown in Scheme **1**. The key intermediate 4,6-di(9H-carbazol-9-yl)isophthalonitrile (**2CzIPN**) was synthesized via a literature protocol in good yield (82%).[38] The nitriles were converted into the corresponding 1,3,4-oxadiazoles following a two-step protocol wherein **2CzIPN** was reacted with ammonium chloride and sodium azide in DMF at 110 °C for 8 h to afford **2CzIT** in an excellent yield of 90%. **2CzIT** was then decomposed in the presence of the corresponding acid chloride in dry pyridine at 110 °C for 12 h to afford the target TADF emitters with yields of 35%, 65%, 75% and 72% for ***i*-2CzdOXDMe**, ***i*-2CzdOXDPh**, ***i*-2CzdOXD4CF$_3$Ph** and ***i*-2CzdOXD4MeOPh**, respectively. The identity and purity of the four compounds were verified by a combination of ^{1}H, ^{13}C and ^{19}F NMR (Figures **S1**−**S16**), melting point, high performance liquid chromatography, high resolution mass spectrometry and elemental analyses. The thermal properties were investigated by thermogravimetric analysis (TGA), differential thermal analysis (DTA) and differential scanning calorimetry (DSC) under a nitrogen atmosphere. As shown in Figure **S24**, ***i*-2CzdOXDMe**, ***i*-**

2CzdOXDPh, ***i*-2CzdOXD4CF$_3$Ph** and ***i*-2CzdOXD4MeOPh**, have very high decomposition temperatures (T_d) of 394, 400, 402 and 402 °C, respectively, while there was no obvious glass transition temperature (T_g) found from DSC traces. ***i*-2CzdOXD4CF$_3$Ph** melts at 325 °C, while ***i*-2CzdOXDMe**, ***i*-2CzdOXDPh** and ***i*-2CzdOXD4MeOPh** melt at 298, 294 and 270 °C, respectively (DTA and DSC traces, see Figures S24-S26). These thermal properties indicate a high potential thermal stability for OLED device fabrication.

Density Functional Theory (DFT) Calculations.

To understand the relationship between molecular structure and the optoelectronics of the four 1,3,4-oxadiazole-based emitters, density functional theory (DFT) and time-dependent density functional theory (TD-DFT) simulations were performed employing the PBE0[46] functional and the Pople[47] 6-31G(d,p) basis set; the Tamm–Dancoff approximation (TDA) was treated as a variant of TD-DFT.[48-49] The ground state structures were first optimized, starting from the single crystal structure geometry where possible. The calculated dihedral angles between the carbazoles and the central benzene in the optimized ground state geometries are 37.43°, 39.52°; 37.51°, 37.76°; 71.14°, 71.15°; 71.82°, 71.83° for ***i*-2CzdOXDMe**, ***i*-2CzdOXDPh**, ***i*-2CzdOXD4CF$_3$Ph** and ***i*-2CzdOXD4MeOPh**, respectively, values that are modestly larger than those calculated for **2CzIPN** with 34.20° to 38.50°. The larger dihedral angles are the result of the increased steric hindrance felt by the carbazoles due to the adjacent oxadiazole units. Their single crystal structures (*vide infra*) have more twisted carbazole donors and hence larger dihedral angles (64.26° to 86.36°) than those in the calculated structures.

Figure **1** shows the calculated HOMO and LUMO electron density distributions and energies along with the energies of the excited S_1 and T_1 states. The HOMOs of the four compounds are expectedly mainly localized on carbazole donors while the LUMOs are localized on the oxadiazole acceptors, with minor contributions from the phenyl bridge. Compared to **2CzIPN** (E_{HOMO} = -6.14 eV) the HOMO energies of the four oxadiazole emitters are all shallower, except ***i*-2CzdOXD4CF$_3$Ph** (-6.17 eV), and range from -5.73 eV to -5.88 eV, values that are likewise destabilized compared to the corresponding HOMO levels for their previously reported 1,2-isomers (-6.09 to -6.15 eV).[35] The LUMO energies vary more widely from -1.87 to -2.32 eV as a function of the different substituents of the oxadiazole acceptors. ***i*-2CzdOXD4CF$_3$Ph**, with 4-trifluoromethylphenyl-modified oxadiazole acceptors, has the deepest LUMO (E_{LUMO} = -2.32 eV) of the four compounds. As expected, the LUMO energies of the four compounds are also higher than their 1,2-isomers, which indicate the oxadiazole-based emitters with donors and acceptors at *ortho*-positions with respect to each other result in higher HOMO and LUMO energy levels than their 1,2-isomers where the two donors and two acceptors are each adjacent to each other. Additionally, in replacing the cyano groups of **2CzIPN** with oxadiazoles, the electron density distribution of the LUMOs become more delocalized and further spatially separated from the donor carbazoles. These results indicate that the substituents on the oxadiazoles and the relative position of the donors and acceptors both play important roles in tuning the HOMO and LUMO energies of these emitters.

The overlap of HOMO and LUMO is small, leading to small calculated ΔE_{ST} of 0.23, 0.25, 0.23 and 0.39 eV for ***i*-2CzdOXDMe**, ***i*-2CzdOXDPh**, ***i*-2CzdOXD4CF$_3$Ph** and ***i*-2CzdOXD4MeOPh**, respectively; the value calculated for **2CzIPN** is comparable with 0.24 eV.

The ΔE_{ST} values of all the four oxadiazole compounds are smaller by 0.02 to 0.13 eV than that of the corresponding 1,2-dioxadiazole isomers where ΔE_{ST} ranged from 0.29 eV to 0.41 eV. Importantly, the HOMO-LUMO transition from the S_1 state shows relatively higher oscillator strengths (*f*) of 0.11-0.15 (Table **S4**) for the four compounds compared to their 1,2-dioxadiazole isomers where *f* ranged from 0.10 to 0.13, which could lead to higher Φ_{PL} values; in each case the S_1 state remains predominantly charge-transfer (CT) in nature.

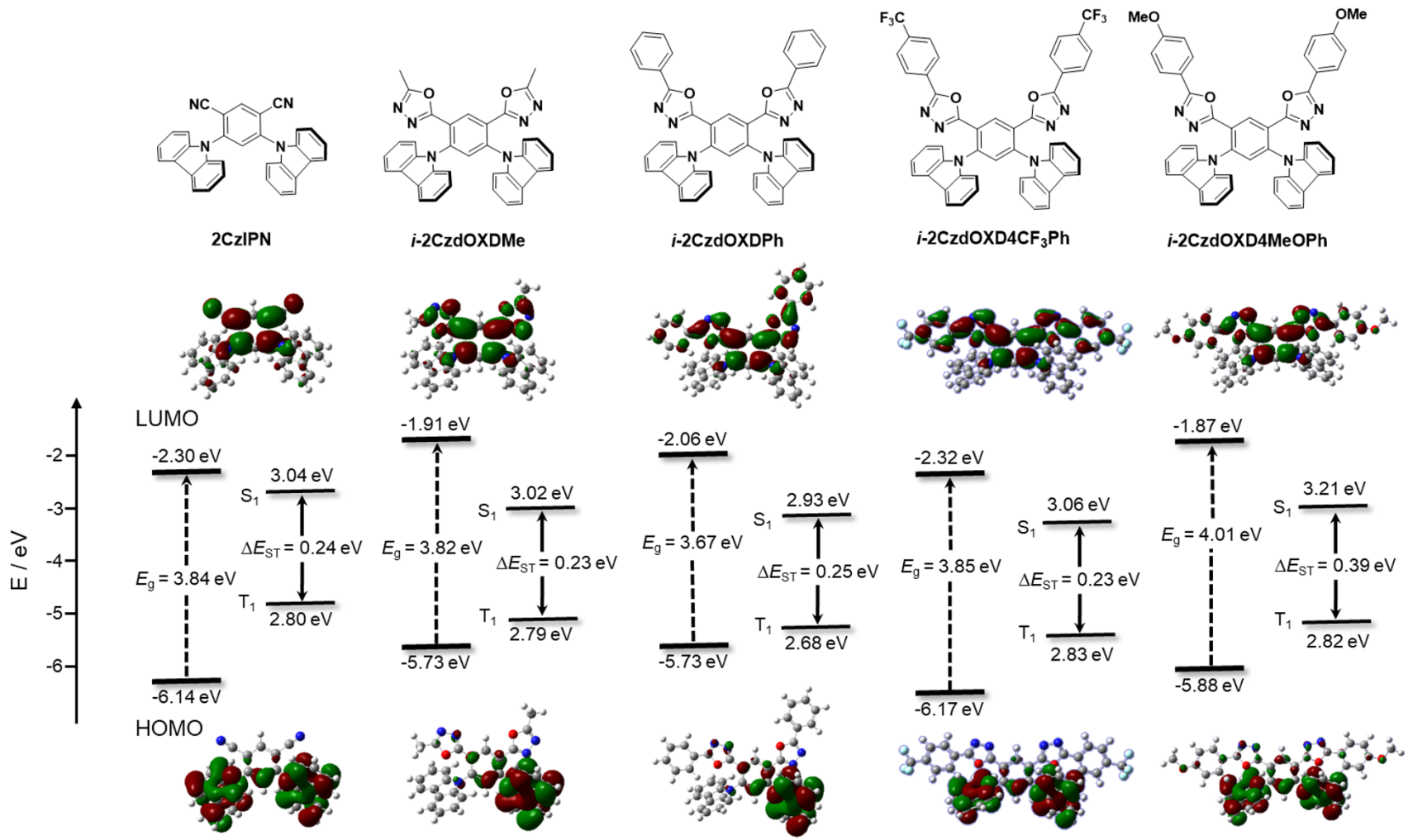

Figure **1**. Molecular structures and HOMO/LUMO distributions of **2CzIPN** and 1,3,4-oxadiazole-based TADF compounds (based on DFT/PBE0/6-31G(d) level theory).

Crystal structures.

Single crystal structures were obtained for all four oxadiazole TADF emitters as well as for the reference compound **2CzIPN** using X-ray diffraction analysis (Figure **2**). Crystals of **2CzIPN, *i*-2CzdOXDPh** and ***i*-2CzdOXD4CF$_3$Ph** were grown by the slow vapor diffusion of diethyl ether into corresponding concentrated solutions of dichloromethane, crystals of ***i*-2CzdOXDMe** were grown by slow evaporation of mixed solution of methanol and dichloromethane, while crystals of ***i*-2CzdOXD4MeOPh** were grown by slow evaporation from mixed solution of toluene and acetonitrile. All the four oxadiazole compounds have similar conformations, with both carbazole donors found in a highly twisted conformation with respect to the plane of central benzene (dihedral angles of 64.26° to 86.36°); the carbazoles are closer to an orthogonal conformation than those found in **2CzIPN** (dihedral angles of 48.94° to 72.32°). Moreover, the carbazole units in the four oxadiazole compounds exhibit much more twisted conformations than those of their 1,2-dioxadiazole isomers (dihedral angles of 58.51° to 67.64°) due to the increased steric hindrance between carbazole donors and oxadiazole acceptors. As a corollary, the oxadiazole moieties are closer to a coplanar conformation with the central benzene (dihedral angles of 2.61° to 24.12°) than their 1,2-dioxadiazole isomers (dihedral angles of 6.18° to 78.11°).

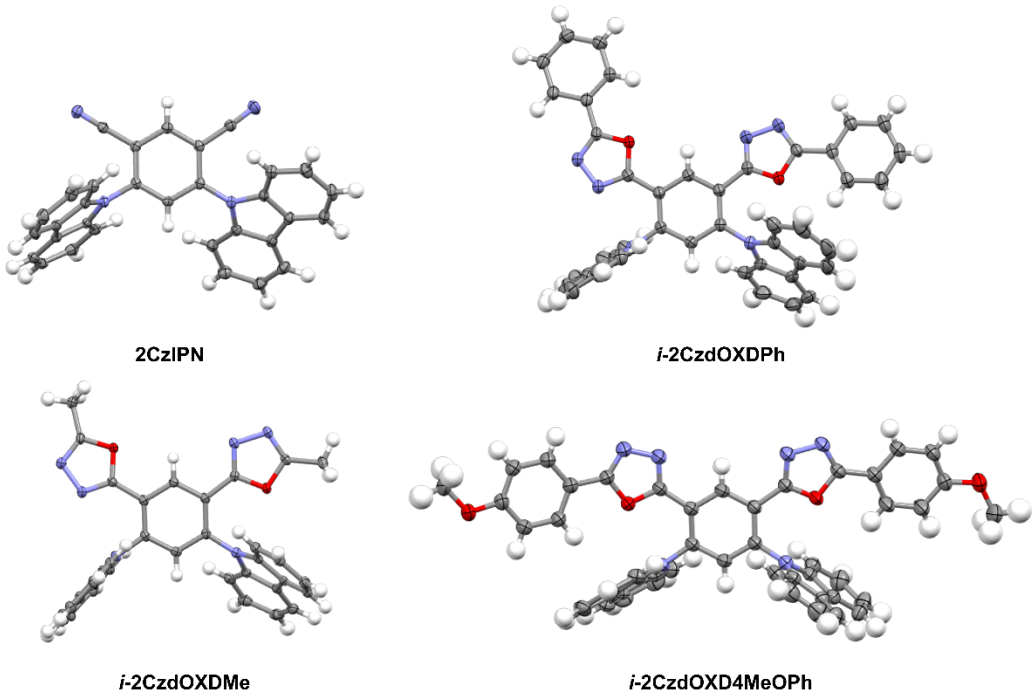

Figure **2.** Crystal structures of **2CzIPN**, ***i*-2CzdOXDMe**, ***i*-2CzdOXDPh** and ***i*-2CzdOXD4MeOPh** (50% probability ellipsoids; co-crystallized solvent molecules omitted). Heteroatoms: N, light blue; and O, red.

Electrochemistry.

The electrochemistry of the four oxadiazole compounds and the reference **2CzIPN** has been studied by cyclic voltammetry (CV) and differential pulse voltammetry (DPV) in degassed acetonitrile (Figure **3**). All five compounds show irreversible carbazole-centred oxidation waves[50] and quasi-reversible oxadiazole-centered reduction waves. The HOMO energy levels, calculated from the onset of the oxidation potential, were found to be -5.75, -5.71, -5.72 and -5.70 eV for ***i*-2CzdOXDMe**, ***i*-2CzdOXDPh**, ***i*-2CzdOXD4CF$_3$Ph** and ***i*-2CzdOXD4MeOPh**, respectively (Table **1**). The almost identical HOMO energy levels are a result of identical donors in the four compounds along with very poor electronic coupling to the acceptor groups; these results are in

line with the DFT calculations, *vide supra*. The slightly shallower HOMO energy levels of these four compounds compared to those of their 1,2-dioxadiazole isomers reflect the reduced conjugation resulting from the increased torsions of the carbazoles; the HOMO energy levels are also slightly shallower than that of **2CzIPN** (E_{HOMO} = -5.84 eV). The HOMO energy levels were also measured for solid films using ambient photoemission spectroscopy (APS) (Figure **S32** and Table **1**). This showed the same trend as the CV measurements though HOMO levels are slightly stabilized, reflecting the influence of the medium in the CV measurements. The HOMO level of **2CzIPN** (-5.98 eV) measured by APS is lower than that of the four oxadiazole TADF emitters where E_{HOMO} = -5.77 eV, -5.75 eV, -5.71 eV and -5.78 eV for ***i*-2CzdOXDMe**, ***i*-2CzdOXDPh**, ***i*-2CzdOXD4CF$_3$Ph** and ***i*-2CzdOXD4MeOPh**, respectively.

The LUMO energy levels calculated from the onset of the reduction potential, were found to be -2.77, -2.85, -2.93 and -2.78 eV for ***i*-2CzdOXDMe**, ***i*-2CzdOXDPh**, ***i*-2CzdOXD4CF$_3$Ph** and ***i*-2CzdOXD4MeOPh**, respectively. The LUMO energy levels of ***i*-2CzdOXDMe**, ***i*-2CzdOXDPh** and ***i*-2CzdOXD4MeOPh** are approximately 0.1 eV shallower compared to that of ***i*-2CzdOXD4CF$_3$Ph** as a result of the relatively increased electron-donating character of the substituents in the three former compounds; ***i*-2CzdOXDMe** has the shallowest LUMO at -2.77 eV while ***i*-2CzdOXD4CF$_3$Ph** has the most stabilized LUMO at -2.93 eV. The LUMO energy levels of the four compounds are more stabilized compared to their 1,2-bis(oxadiazole) isomers (by 0.04 to 0.07 eV), which is due to the decreased conjugation present in the former because of their more twisted conformations. As expected, the replacement of the nitrile groups with 1,3,4-oxadiazoles results in shallower LUMO energy levels than that of **2CzIPN** (E_{LUMO} = -2.96 eV).

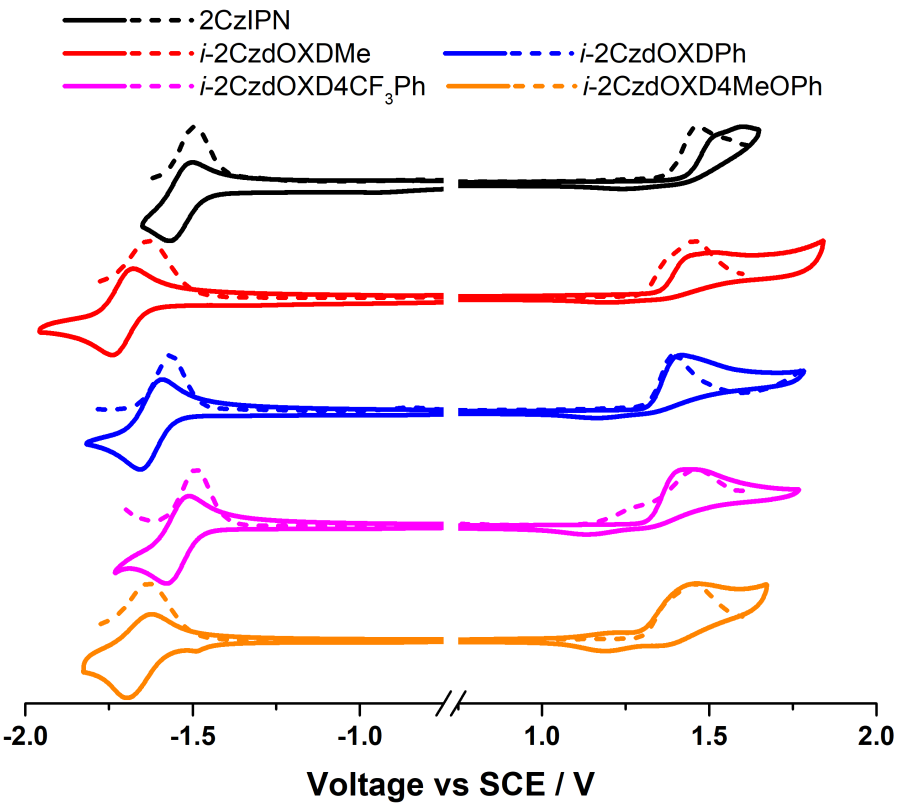

Figure **3**. CV (solid) and DPV (dashed) traces for **2CzIPN** and the four oxadiazole-based emitters in degassed MeCN under nitrogen with 0.1 M [*n*Bu$_4$N]PF$_6$ as the supporting electrolyte and using Fc/Fc$^+$ as the internal standard. Scan rate = 100 mV/s.

Table **1**. Summary of decomposition temperature, solution-state optoelectronic characterization and APS data for **2CzIPN** and 1,3,4-oxadiazole-based TADF emitters.

Emitter	T_d[a] / °C	λ_{abs}[b] / nm [$\varepsilon \times 10^{-3}$ / M^{-1} cm^{-1})]	E_g[c] / eV	λ_{PL}[d] / nm	Φ_{PL}[e] / %	τ_p[f] / ns	τ_d[f] / μs	HOMO[g] / eV	LUMO[g] / eV	HOMO[h] / eV
2CzIPN	-	286[3.38] 315[1.22] 329[1.51] 374[1.45]	3.01	454	-	9.0	5.5	-5.84	-2.96	-5.98
i-2CzdOXDMe	397	256[4.94] 279[2.21] 288[2.28] 322[1.35] 333[1.63] 359[1.06]	3.17	444	6.8 (6.9)	6.5	-	-5.75	-2.77	-5.77
i-2CzdOXDPh	400	255[2.42] 279[3.05] 289[4.04] 303[2.73] 333[1.31] 370[0.77]	3.15	439	10.1 (9.9)	4.9	-	-5.71	-2.85	-5.75
i-2CzdOXD4CF$_3$Ph	402	255[4.22] 281[6.03] 289[6.78] 307[3.86] 332[1.85] 376[1.08]	3.06	456	9.5 (8.8)	5.1	-	-5.72	-2.93	-5.71
i-2CzdOXD4MeOPh	402	257[4.04] 289[4.78] 320[5.29] 332[4.42] 371[1.38]	3.17	428	13.3 (13.1)	5.1	-	-5.70	-2.78	-5.78

[a] From 5% weight loss temperature by TGA at 10 °C min^{-1}. [b] in toluene at 298 K, [c] E_g calculated from the onset of UV-vis absorption spectra. [d] Measured in 10^{-5} M toluene solution at room temperature. λ_{exc} = 360 nm. [e] Measured in 10^{-5} M degassed toluene solution at room temperature. Values in parentheses are for aerated solutions. 0.5 M quinine sulfate in H_2SO_4 (aq) was used as reference (Φ_{PL}: 54.6%).[51] [f] PL lifetimes of prompt (τ_p) and delayed (τ_d) decay components for degassed toluene solution measured at room temperature λ_{exc} = 360 nm. [g] in MeCN with 0.1 M [nBu$_4$N]PF_6 as the supporting electrolyte and Fc/Fc^+ as the internal reference. The HOMO and

LUMO energies were calculated using the relation $E_{HOMO/LUMO} = -(E^{ox}_{pa,1}/ E^{red}_{pc,1} + 4.8)$ eV, where E^{ox}_{pa} and E^{red}_{pc} are anodic and cathodic peak potentials, respectively.[52] [h] Calculated from APS spectra.

Photophysical properties.

The UV-vis absorption and photoluminescence spectra of the four 1,3,4-oxadiazole compounds and **2CzIPN** were recorded at 298 K in toluene (Figure **4a**, Table **1**), diethyl ether, dichloromethane, tetrahydrofuran, ethyl acetate, chloroform and acetonitrile (Figures **S27-S28**). All five compounds exhibit similar absorption profiles in toluene. The strongly absorptive bands below 350 nm are attributed to the π-π^* absorption transitions while the weaker absorption bands between 350-420 nm are assigned to intramolecular charge transfer (ICT) transitions between the carbazole donors and oxadiazole acceptors. The TD-DFT simulated UV-vis absorption spectra (Figure **S34**) match well to experiment. The optical gaps, E_g, (Table **1**) of ***i*-2CzdOXDMe**, ***i*-2CzdOXDPh, *i*-2CzdOXD4CF$_3$Ph** and ***i*-2CzdOXD4MeOPh**, calculated from the intersection point of the normalized absorption and emission spectra, are 3.17, 3.13, 3.06 and 3.02 eV, respectively, which are higher by 0.04-0.14 eV compared with that of **2CzIPN** (E_g = 3.01 eV). The trends observed in E_g as well as the wavelength of maximum absorption, λ_{abs}, for the ICT band are consistent with the electronic character of the substituent on the oxadiazole acceptors and follow the trend in LUMO energies and redox gaps observed by electrochemistry. For instance, ***i*-2CzdOXD4CFCF$_3$Ph** has the most stabilized LUMO energy level and the correspondingly smallest E_g of 3.06 eV of the four oxadiazole emitters. The UV-vis absorption spectra of the emitters in various solvents with different polarity are shown in Figure **S27**. All four TADF emitters showed a red-shift of absorption with increasing solvent polarity, which is consistent with the lowest band being ICT in nature.

All four compounds show blue emission in toluene with the wavelength of maximal emission, λ_{PL}, at 428 nm, 439 nm, 444 nm and 456 nm for ***i*-2CzdOXD4MeOPh**, ***i*-2CzdOXDMe**, ***i*-**

2CzdOXDPh and ***i* -2CzdOXD4CF$_3$Ph**, respectively. The trends in λ_{PL} mirror those in E_g. The emission of the four compounds was blue-shifted by 14-31 nm (704-1578 cm^{-1}) compared with their 1,2-dioxadiazole isomers, which is consistent with the theoretical calculations. The photoluminescence (PL) spectra of each of the four compounds exhibit strong positive solvatochromism (Figure **S28**) and become broader with increasing solvent polarity, with the full width at half maxima (FWHM) changing from about 70 nm in diethyl ether to about 95 nm in acetonitrile. These results clearly indicate that the emission of the four compounds is ICT in nature.

The time-resolved PL of **2CzIPN** and the four oxadiazole emitters in toluene are shown in Figure **4b**. The emission lifetime (Table **1**) of **2CzIPN** shows biexponential decay kinetics and consists of prompt, τ_p, (9.0 ns, 61.1%) and delayed, τ_d, (5.5 μs, 38.9%) components. By comparison, the prompt PL decay of the four oxadiazole compounds is slightly faster, with τ_p values of 6.5 ns, 4.9 ns, 5.1 ns and 5.1 ns for ***i*-2CzdOXDMe**, ***i*-2CzdOXDPh**, ***i*-2CzdOXD4CF$_3$Ph** and ***i*-2CzdOXD4MeOPh**, respectively. The τ_p values of these compounds are also much shorter than those of their 1,2-dioxadiazole isomers. In solution, the delayed decay component is too weak to be resolved, a behavior similar to that observed in our previous report.

The photoluminescence quantum yields (Φ_{PL}) in degassed toluene are low and range from 7-13% (Table **1**). There is essentially no change when measured under aerated conditions suggesting that in toluene these compounds behave as fluorescent emitters; this is a similar behavior to our previously reported oxadiazole emitters.[35] To investigate the TADF characteristics of the four compounds in the solid state, the PL emission of 10 wt% PMMA films in air and

vacuum conditions also have been recorded (Figure **S29**). The Φ_{PL} of 10 wt% PMMA thin films (Table **2**) are 38%, 41%, 52% and 28% for ***i*-2CzdOXDMe**, ***i*-2CzdOXDPh**, ***i*-2CzdOXD4CF$_3$Ph** and ***i*-2CzdOXD4MeOPh**, respectively. The Φ_{PL} measured under air was typically less than half of the value measured under N_2 due to PL quenching by oxygen. The emission spectra in 10 wt% PMMA films are shown in Figure **4c**. The emission spectra are red-shifted for ***i*-2CzdOXDMe** (7 nm, 445 cm^{-1}) and ***i*-2CzdOXD4MeOPh** (8 nm, 492 cm^{-1}) compared to their 1,2-oxadiazole isomers but the other two compounds are blue-shifted for ***i*-2CzdOXDPh** (3 nm, 183 cm^{-1}) and ***i*-2CzdOXD4CF$_3$Ph** (8 nm, 457 cm^{-1}) compared to their respective isomers. This result suggests that the four oxadiazole compounds could possess TADF properties.

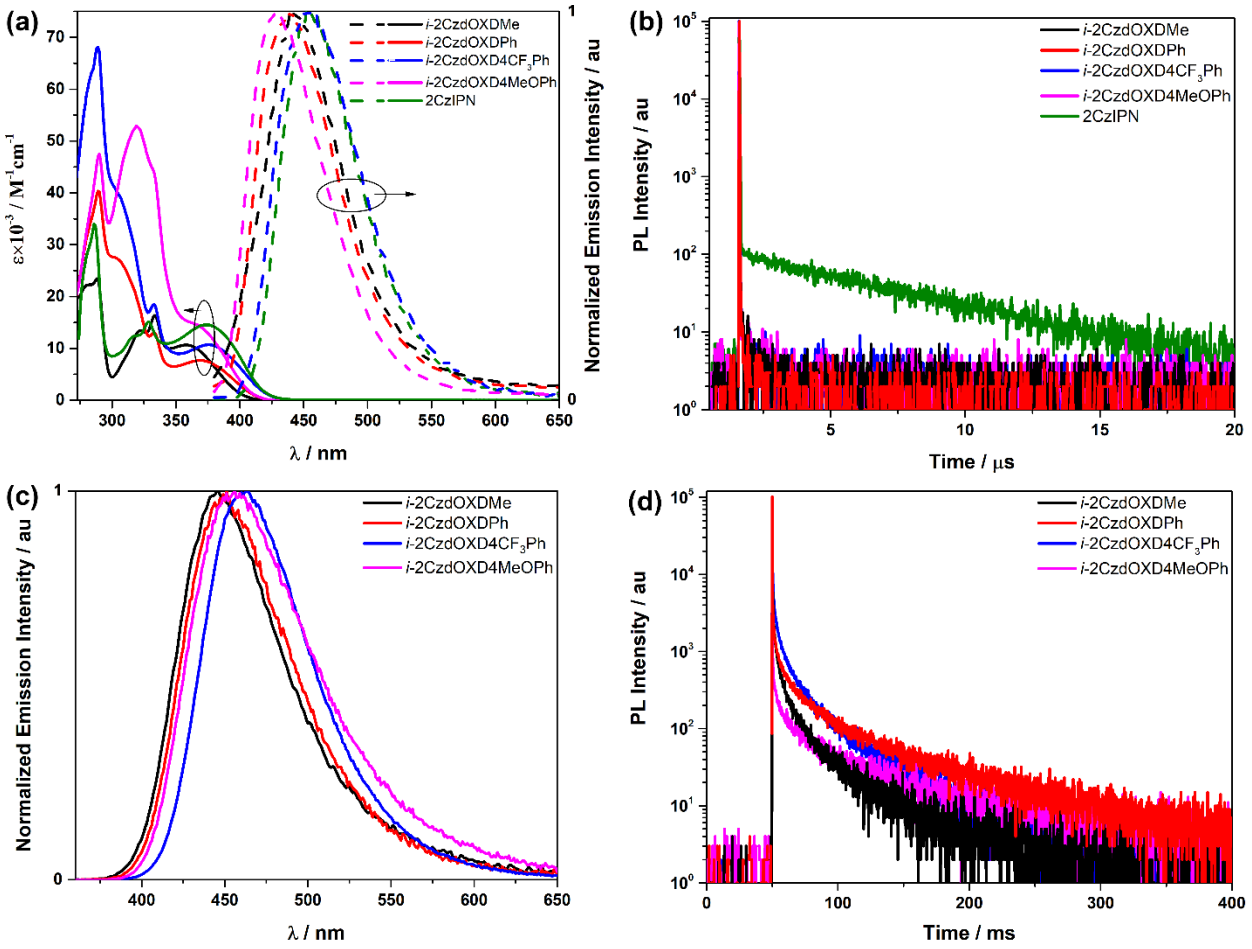

Figure **4**. a) UV−vis absorption and PL spectra (λ_{exc} = 360 nm) of 10^{-5} M oxadiazole emitters in toluene solution at 298 K; b) time-resolved PL spectra (λ_{exc} = 360 nm) in degassed toluene solution (10^{-5} M) at 298 K; c) steady-state PL spectra (λ_{exc} = 340 nm) of 10 wt% doped PMMA films under vacuum and d) time-resolved PL spectra (λ_{exc} = 340 nm) of 10 wt% doped PMMA films under vacuum.

The time-resolved PL of 10 wt% PMMA doped films are shown in Figure **4d**, and all consist of a fast prompt decay (τ_p, 6.3 - 8.6 ns) and several very long delayed decay components, τ_d (Tables **2** and **S3**). The average lifetime of the delayed decay was calculated to be 24.6 ms, 58.6 ms, 31.5 ms and 64.9 ms for ***i*-2CzdOXDMe**, ***i*-2CzdOXDPh**, ***i*-2CzdOXD4CF$_3$Ph** and ***i*-**

2CzdOXD4MeOPh, respectively. The TADF emitters in this work possess a faster prompt decay than their 1,2-isomers ($\tau_p \approx 11$ ns). For the delayed lifetimes, all are in the millisecond range and are longer than their respective 1,2-isomers with the exception of ***i*-2CzdOXDMe**, which has a shorter delayed lifetime ($\tau_{avg} = 24.6$ ms) than its isomer, **2CzdOXDMe**, $\tau_{avg} = 33.2$ ms.

Table 2. Photophysical properties of doped films.

Emitter	PMMA			DPEPO			ΔE_{ST}[d] / eV	ΔE_{ST}[e] / eV
	λ_{PL}[a]/nm	Φ_{PL}[b]/%	τ_{avg} /ns[c]	λ_{PL}[a]/nm	Φ_{PL}[b]/%	τ_{avg} /ns[c]		
***i*-2CzdOXDMe**	443	37.7 (17.4)	7.4; 24.6 $\times 10^6$	448	59.0 (19.3)	8.5; 48.3 $\times 10^6$	0.31	0.23
***i*-2CzdOXDPh**	445	41.3 (19.5)	6.3; 58.6$\times 10^6$	459	58.1 (19.7)	8.6; 55.1$\times 10^6$	0.31	0.25
***i*-2CzdOXD4CF3Ph**	458	51.7 (20.2)	8.6; 31.5$\times 10^6$	480	69.8 (24.3)	8.6; 97.9$\times 10^6$	0.32	0.23
***i*-2CzdOXD4MeOPh**	442	27.6 (17.5)	7.0; 64.9$\times 10^6$	452	35.4 (18.6)	7.3; 110.2 $\times 10^6$	0.44	0.39

[a] Emission maxima is reported from doped films in vacuum. Thin films were prepared by spin-coating doped samples in PMMA (10 wt%) or DPEPO (10 wt%). [b] Values determined using an integrating sphere under an N_2 atmosphere. Values in parentheses are for samples measured in air. [c] Prompt lifetimes determined from the monoexponential or biexponential fit of the initial decay by TCSPC; delayed lifetimes determined from the triexponential decay by MCS. The average lifetime in this table was calculated using $\tau_{avg} = \sum A_i\tau_i^2/\sum A_i\tau_i$, where A_i is the pre-exponential factor for lifetime τ_i.[20] [d] ΔE_{ST} was determined from the difference between the onset of the singlet and triplet emission measured with a gated iCCD detector. [e] Calculated from TD-DFT at the standard Pople 6-31G (d, p) level.

We continued our studies of films by measuring the emitters in high triplet energy hosts DPEPO (E_T = 3.1 eV[53]) and PPT (E_T = 3.0 eV[54]). The thin film Φ_{PL} in 10 wt% PPT and DPEPO are summarized in Table **2**. In contrast to the measurements above, typically much higher Φ_{PL} values were found, ranging from 37-59%, in 10 wt% DPEPO films and 35%-70% in 10 wt% PPT films. As with the measurements in PMMA, the four oxadiazole compounds show TADF in these polar hosts. The Φ_{PL} of **2CzIPN** in 10 wt% DPEPO is much higher than those of the four oxadiazole-based TADF emitters at 82% and 68% for measurements under vacuum and air conditions, respectively.

The emission in 10 wt% doped films in DPEPO (Figure **5a**) remained broad and unstructured with maxima slightly red-shifted compared to those in toluene at 448 nm, 459 nm, 480 nm and 452 nm for ***i*-2CzdOXDMe**, ***i*-2CzdOXDPh**, ***i*-2CzdOXD4CF$_3$Ph** and ***i*-2CzdOXD4MeOPh**, respectively. The PL characteristics in 10 wt% doped films in PPT (Figure **5b**) are essentially the same as in DPEPO. The time-resolved PL decay traces of the DPEPO doped films at room temperature are shown in Figure **5c** and summarized in Table **2**. Similar to the behavior in PMMA, there are both prompt and delayed emission components. In each case, the prompt PL decay can be best modelled with two components while the delayed PL decay is triexponential. All four emitters have very long millisecond τ_d, which is much longer than their 1,2-isomers in the previous report. ***i*-2CzdOXD4MeOPh** exhibits the longest average decay lifetime of 110.2 ms, followed by ***i*-2CzdOXD4CF$_3$Ph** (97.9 ms), ***i*-2CzdOXDPh** (55.1 ms) and ***i*-2CzdOXDMe** (48.3 ms). The energy gap between singlet and triplet (ΔE_{ST}) was calculated from the difference in the onset of fluorescence and phosphorescence spectra recorded at 77 K (Figure **5d** and Table **2**). The locally excited (^{3}LE) nature of T_1 states of these four emitters were assigned

based on the low temperature structured phosophorescence spectra, and are centered on the oxadiazole moieties. There are correspondingly larger ΔE_{ST} values of 0.31 eV, 0.31 eV, 0.32 eV and 0.44 eV for ***i*-2CzdOXDMe**, ***i*-2CzdOXDPh**, ***i*-2CzdOXD4CF$_3$Ph** and ***i*-2CzdOXD4MeOPh**, respectively, than that of the reference **2CzIPN** (0.10 eV). The corresponding reverse intersystem crossing rates (k_{RISC}) at 300 K are much lower than that of **2CzIPN** as inferred from the slower decay of the PL (Figure **6**).

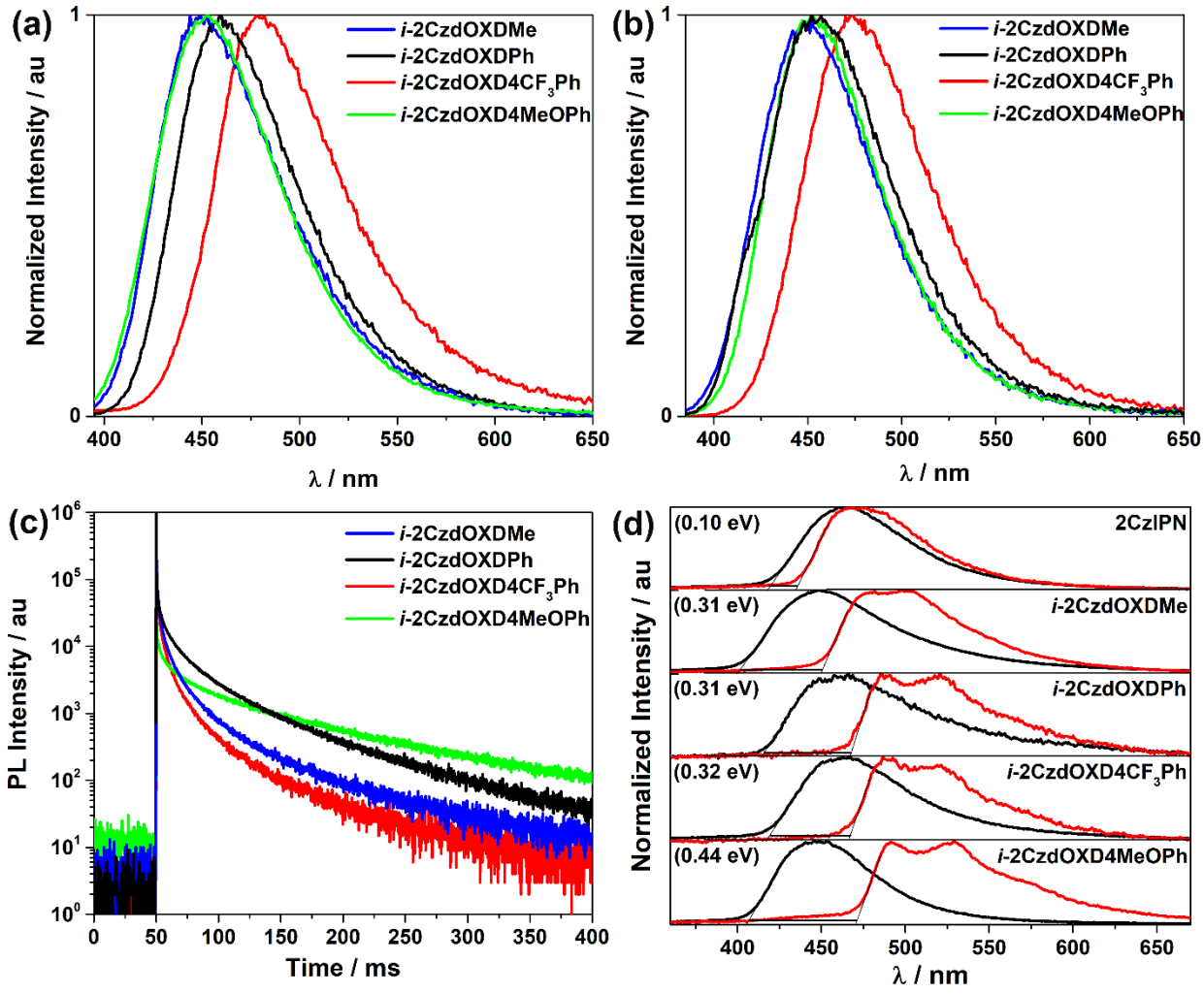

Figure **5**. Normalized emission spectra (λ_{exc} = 360 nm) of 10 wt% doped **a**) DPEPO films and **b**) PPT films. **c**) time-resolved PL spectra (λ_{exc} = 360 nm) of 10 wt% doped DPEPO films. **d**) Prompt

(red) and delayed (black) PL spectra of 10 wt% doped DPEPO films at 77 K. Values in parentheses are ΔE_{ST}.

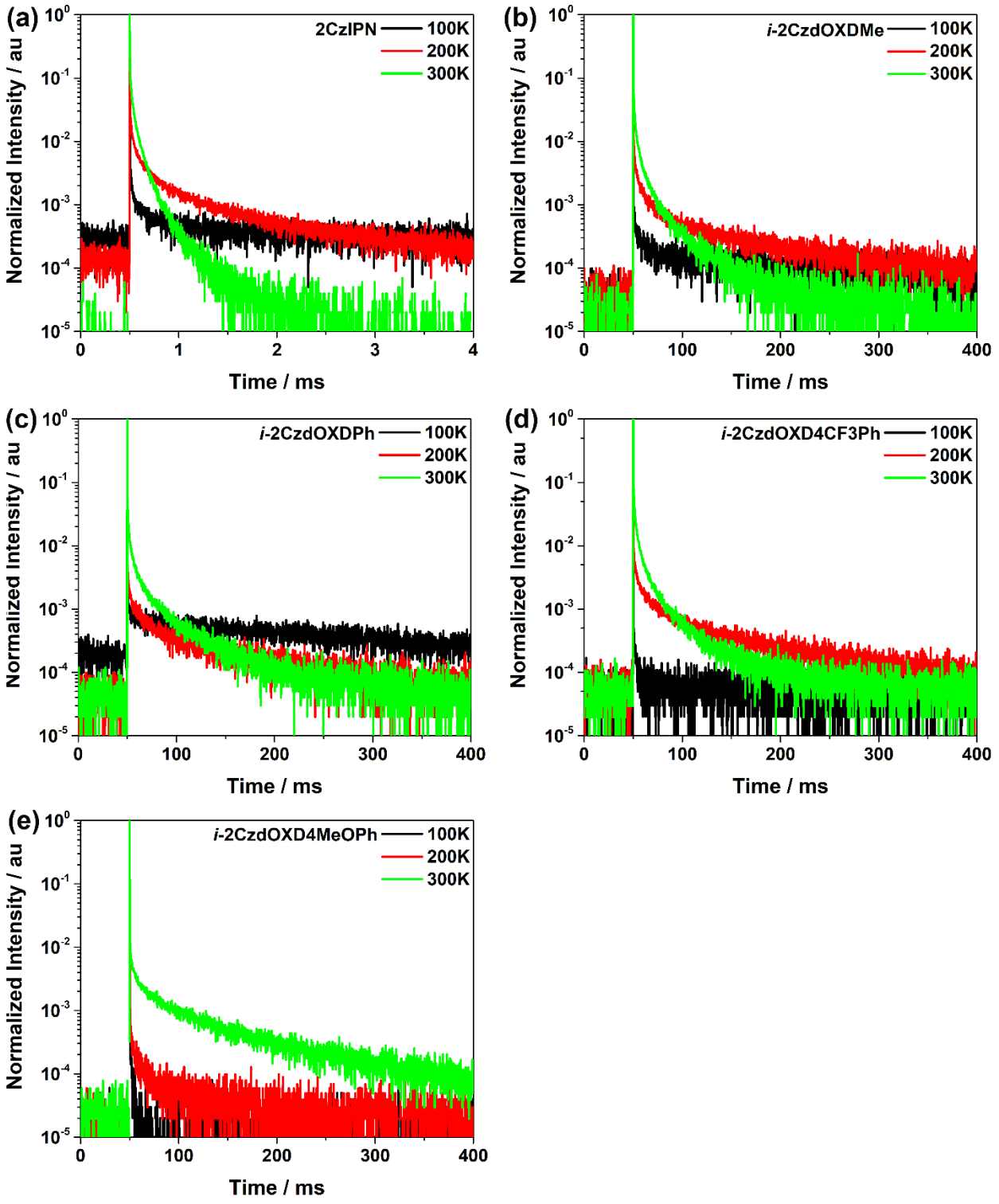

Figure **6**. Temperature-dependent time-resolved PL (λ_{exc} = 378 nm, λ_{det} = 460 nm) in 10 wt% doped films in DPEPO under vacuum for a) **2CzIPN**, b) ***i*-2CzdOXDMe**, c) ***i*-2CzdOXDPh**, d) ***i*-2CzdOXD4CF$_3$Ph**, e) ***i*-2CzdOXD4MeOPh**.

The temperature dependent time-resolved PL are shown in Figure **6**. The magnitude of the delayed component tended to increase with increasing temperature from 100K to 300K, thereby demonstrating the essential role of thermal activation in the promotion of the delayed fluorescence.

Dipole moment orientation

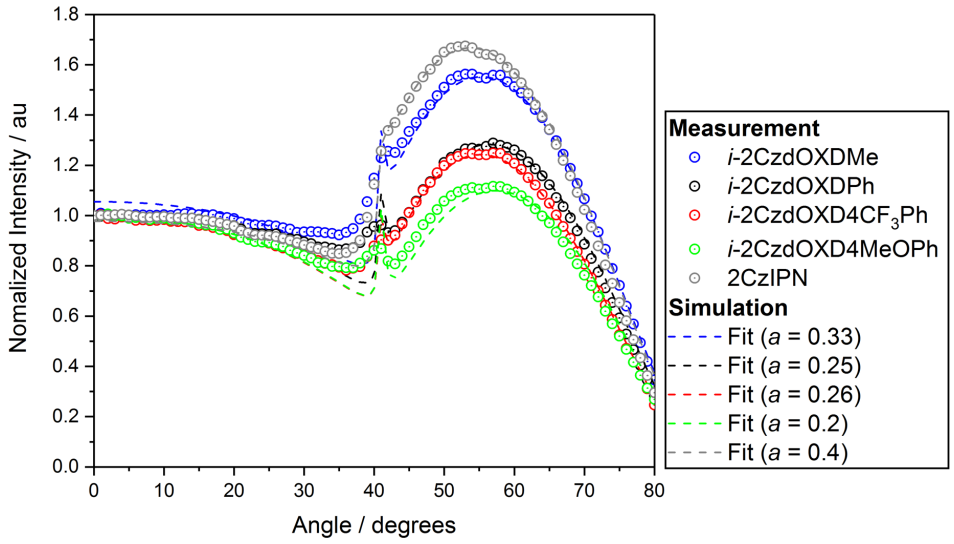

Figure **7**. Angle-dependent PL intensity at the peak emission wavelength of thin films of the four TADF emitters and of the 2CzIPN reference, each doped into DPEPO at 10 wt%. The dashed lines represent the simulated results for the best fit to the measurements data (dots). The corresponding anisotropy factors *a* for each material are indicated in the legend. All data sets were normalized to the intensity of the corresponding curves measured at 0°.

Next, we investigated the average orientation of the transition dipole moments of the four TADF emitters in thin-films. As the dipole orientation of emitters in the EML plays a significant role in the outcoupling efficiency of OLEDs,[55-57] understanding correlation between the molecular orientation and molecular structure is important in order to design TADF emitters with maximized OLED efficiency. Generally, horizontal orientation of the transition dipole moments is favorable in terms of outcoupling efficiency. The dipole orientation of emitters doped into the host can be determined by measuring angle-dependent PL spectra and comparing experimental data with optical simulations (see Supporting Information for details).[58] Figure **S35a** shows a representative example of how the best fit to experimental PL spectra recorded in 1° viewing angle steps is used to find dipole orientation for ***i*-2CzdOXD4CF$_3$Ph**. The result is quantified as the anisotropy factor a, which is defined as the ratio of the number of vertically oriented dipoles to the total number of dipoles; for isotropic orientation when 1/3 of the transition dipole moments are aligned perpendicular to the substrate, $a = 0.33$ while $a = 0$ in the case of perfect horizontal orientation.

Although actual fitting was performed across the full emission wavelength range as illustrated in Figure **S35a**, for simplicity, Figure **7** shows the angle-resolved PL intensities and the simulated best fits to the corresponding measurement only for the peak emission wavelength of each emitter. ***i*-2CzdOXDMe** showed almost isotropic orientation ($a = 0.33$) while preferential horizontal orientation was observed in ***i*-2CzdOXDPh** and ***i*-2CzdOXD4CF$_3$Ph** with $a = 0.25$ and $a = 0.26$, respectively (see Figure **S35b** for a comparison to simulation data assuming isotropic and perfect horizontal orientation). Among the four oxadiazole-based emitters studied here, ***i*-**

2CzdOXD4MeOPh exhibited the most pronounced horizontal orientation with a = 0.2. Interestingly, the dipoles of **2CzIPN** are preferentially vertically oriented (a = 0.4), which means that replacing the cyano groups of **2CzIPN** with oxadiazole acceptors indeed induces a more preferential orientation in terms of efficient light extraction. The nature of the aryl substituent also influences the orientation, with, gratifyingly, electron-rich aryl groups promoted more horizontally aligned emitters as well as bluer emission. The same tendency was observed with the 1,2-oxadiazole TADF emitter series that we reported previously[35] (Figure **S35c**). Specifically, **2CzdOXDMe**, **2CzdOXDPh**, **2CzdOXD4CF$_3$Ph**, and **2CzdOXD4MeOPh** showed anisotropy factors of 0.28, 0.27, 0.27, and 0.22, respectively.

OLED performance

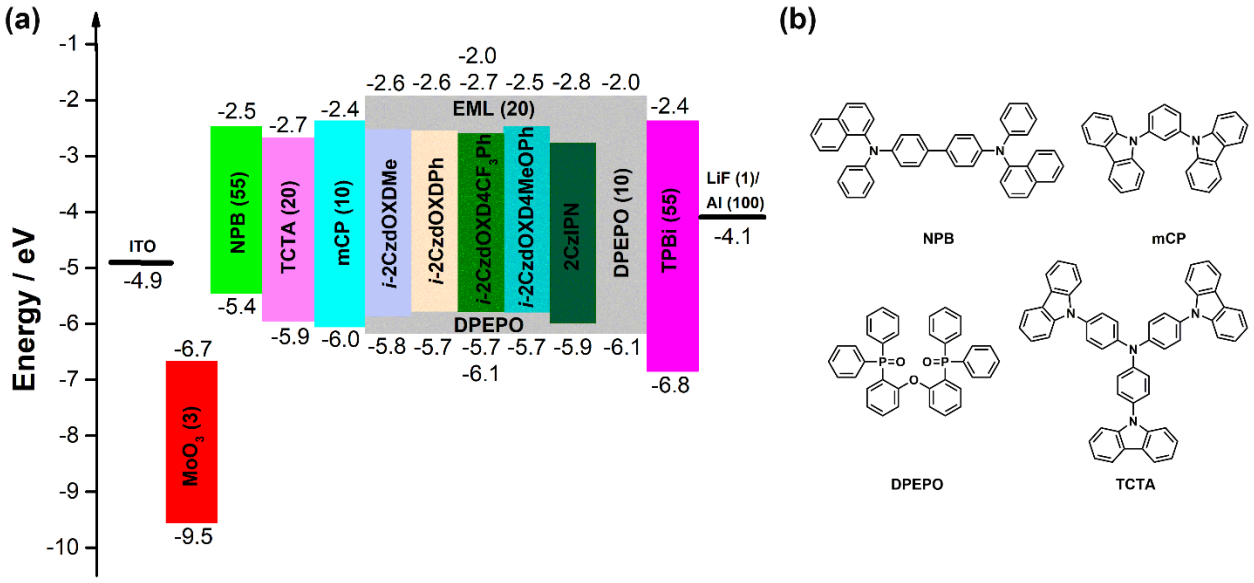

Figure **8**. a) OLED device structure and a proposed energy level diagram; values in parentheses indicate the thicknesses of the corresponding layers (in nm). b) the chemical structure of the materials used in the TADF devices.

Finally, multilayer OLED devices based on the four new emitters were fabricated, using the OLED stack architecture illustrated in Figure **8a**. Specifically, the optimized device has the architecture of: ITO (90 nm)/MoO_3 (3 nm)/NPB (35 nm)/TCTA (20 nm)/mCP (10 nm)/emitter: DPEPO (10 wt %, 20 nm)/DPEPO (10 nm)/TPBi (55 nm)/LiF (1 nm)/Al (100 nm). Molybdenum trioxide (MoO_3) was used as the hole injection layer, *N,N'*-bis(naphthalen-1-yl)-*N,N'*-bis(phenyl)benzidine (NPB) and 4,6-bis(3,5-di(pyridin-3-yl)phenyl)-2-methylpyrimidine (TPBi) were used as the hole transport layer (HTL) and electron transport layer (ETL), respectively. 1,3-di(9H-carbazol-9-yl)benzene (mCP) and (oxybis(2,1-phenylene))bis(diphenylphosphine oxide) (DPEPO) were used as electron and hole blocking layers, respectively. The EML of the devices consisted of the TADF emitters in DPEPO at 10 wt% doping. DPEPO was used as the host because of the appropriate HOMO (-6.1 eV) and LUMO (-2.0 eV) energy levels coupled with its high E_T = 3.1 eV[54] (Table **3**).

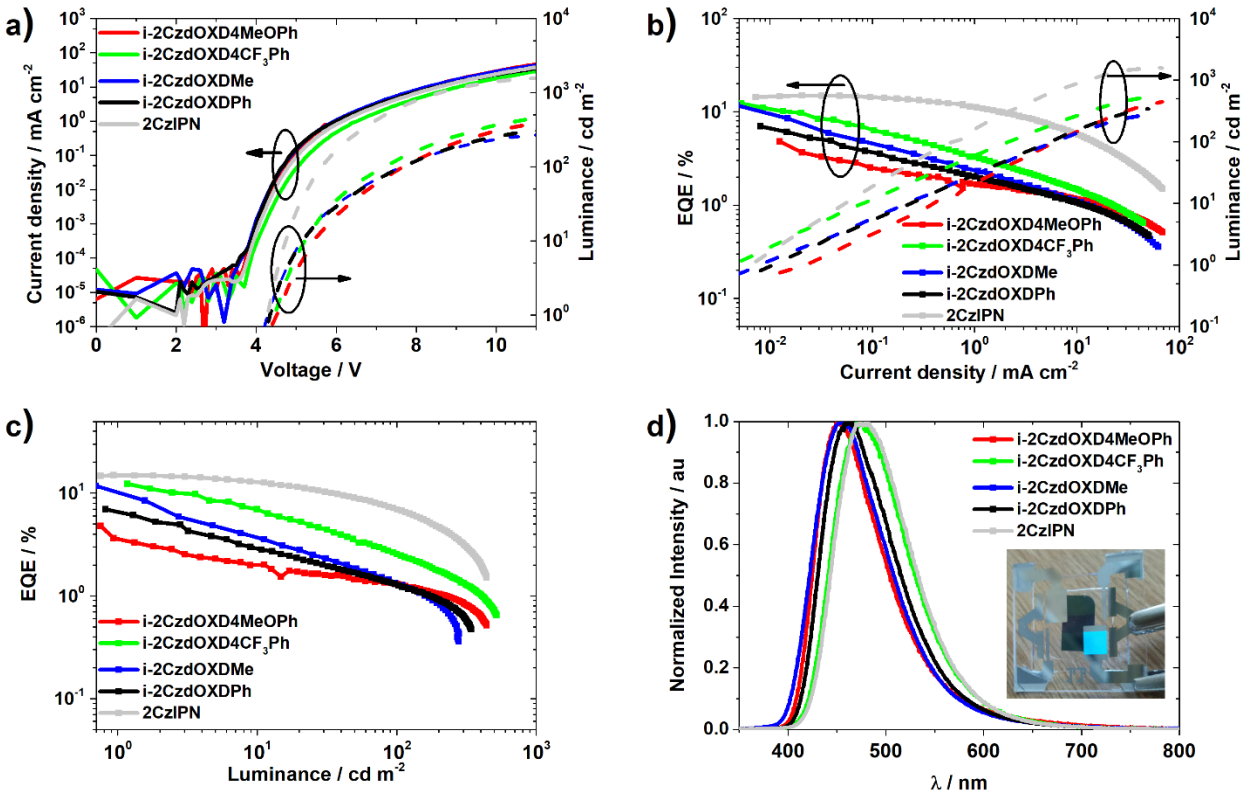

Figure **9**. Performance of OLEDs based on the four emitters studied in this work and of reference OLED based on **2CzIPN**. a) Current density and luminance versus voltage (J–V–L) characteristics. b) EQE and luminance versus current density (EQE-J-L) curves. c) EQE versus luminance (EQE-L) curves. d) EL spectra. Inset shows a photograph of an OLED device based on ***i*-2CzdOXD4CF$_3$Ph** with one of its four pixels operated.

Figure **9** and Table **3** summarize the OLED performance. The devices with ***i*-2CzdOXDMe**, ***i*-2CzdOXDPh**, ***i*-2CzdOXD4CF$_3$Ph** and ***i*-2CzdOXD4MeOPh** exhibited deep blue to sky-blue emission with maxima at 452 nm, 460 nm, 472 nm and 452 nm, respectively (Figure **9d**), which are consistent with their PL emission spectra in DPEPO. Compared to the device with **2CzIPN**, the four oxadiazole-based devices show blue-shifted EL spectra. The FWHM of the EL spectra of ***i*-2CzdOXDMe**, ***i*-2CzdOXDPh**, ***i*-2CzdOXD4CF$_3$Ph** and ***i*-2CzdOXD4MeOPh** are 85 nm, 84 nm, 88 nm and 78 nm, respectively, which are smaller than that of **2CzIPN** (89 nm), thereby providing a purer blue emission. The CIE coordinates for three of the oxadiazole emitters (Table **3**) reveal deep-blue emission with $CIE_{x,y}$ smaller than 0.2 for ***i*-2CzdOXDMe**, ***i*-2CzdOXDPh** and ***i*-2CzdOXD4MeOPh**.

As expected from the Φ_{PL} measurements (Table **2**) and the dipole orientation study (Figure **7**), the OLED with ***i*-2CzdOXD4CF$_3$Ph** reaches the highest maximum external quantum efficiency, EQE_{max}, of 12.3% among the oxadiazole-based OLEDs studied here. The device with ***i*-2CzdOXDMe** showed an EQE_{max} of 11.8% while that with ***i*-2CzdOXDPh** showed an EQE_{max} of 7.0% and with ***i*-2CzdOXD4MeOPh** the EQE_{max} was 4.8%. Although ***i*-2CzdOXD4MeOPh** showed the most promising dipole orientation in terms of the outcoupling efficiency, this was more

than canceled out by the relatively low Φ_{PL} and large ΔE_{ST}. The reference blue OLED with similar CIE coordinates of (0.18, 0.30) based on **2CzIPN** showed an EQE_{max} of 15.0%, which is slightly lower than that of the previous report of 16.4%.[38] These high EQE_{max} values indicate that an efficient triplet harvesting process via a TADF mechanism exists in these OLEDs. However, all OLEDs suffer from severe efficiency roll-off to 7.0%, 1.3%, 1.3%, 2.6% and 1.3% at 100 cd/m^2 for **2CzIPN**, ***i*-2CzdOXDMe**, ***i*-2CzdOXDPh**, ***i*-2CzdOXD4CF$_3$Ph** and ***i*-2CzdOXD4MeOPh**, respectively. Strong efficiency roll-off is expected as all the four new emitter have long τ_d. Compared with our previous report, the OLEDs in this work show much higher EQE_{max} but this is coupled with a more serious efficiency roll-off. Other deep-blue TADF OLEDs employing emitters such as Ac−3MHPM[24] (EQE_{max} = 17.8%, EQE_{100} = 10.4%), MXAc-PM[26] (EQE_{max} = 14,3%, EQE_{100} = 8.4%), Ac-PM[26] (EQE_{max} = 11.4%, EQE_{100} = 5.4%), and 2DPAc-MPM[25] (EQE_{max} = 19.0%, EQE_{100} = 9.4%) possess similar CIE coordinates to our oxadiazole-based TADF OLEDs; however, all show more than 40% efficiency roll-off at 100 cd/m^2 and have relatively long exciton lifetimes.

Table 3. Summarized OLED device performance of **2CzIPN** and oxadiazole-based TADF emitters.

Emitter	λ_{EL} / nm	FWHM / nm	V_{on}[a] / V	EQE_{max}; EQE_{100}[b] / %	η_c / cd A^{-1}	η_p / lm W^{-1}	CIE (x, y)
2CzIPN	477	89	4.3	15.0; 7.0	27.05	19.76	(0.18, 0.30)
***i*-2CzdOXDMe**	452	85	4.33	11.8; 1.3	14.54	10.88	(0.17, 0.17)
***i*-2CzdOXDPh**	460	84	4.3	7.0; 1.3	10.12	7.39	(0.15, 0.16)
***i*-2CzdOXD4CF$_3$Ph**	472	88	4.5	12.3; 2.6	22.31	15.57	(0.18, 0.28)
***i*-2CzdOXD4MeOPh**	452	78	4.5	4.8; 1.3	6.02	4.30	(0.17, 0.17)

[a] Defined as the lowest operating voltage at a luminance of > 1 cd m^{-2}. [b] Max = maximum value, 100 = measured at 100 cd m^{-2}.

CONCLUSIONS

Our motivation in this study was to expand our understanding of the design of blue-emitting materials, and to this end, to explore the use of oxadiazole acceptors in TADF emitter design. We had hypothesized that in a similar manner that **2CzIPN** emits at higher energy than **2CzPN**, a new series TADF emitters, ***i*-2CzdOXDMe**, ***i*-2CzdOXDPh**, ***i*-2CzdOXD4CF$_3$Ph** and ***i*-2CzdOXD4MeOPh**, with substituted 1,3,4-oxadiazole acceptor units would show a deeper blue emission compared to our previously reported oxadiazole-containing emitters with similar regiochemistry to **2CzPN**. Compared with **2CzIPN**, the four TADF emitters all show blue-shifted PL and EL due to the replacement of cyano acceptors by the more weakly electron-withdrawing oxadiazole acceptors. The TADF nature of these emitters was confirmed by PL emission spectra of PMMA and DPEPO doped films, oxygen-dependence on the Φ_{PL} and variable temperature time-resolved PL measurements. OLEDs based on ***i*-2CzdOXDMe** present deep-blue emission with CIE coordinates of (0.17, 0.17) and an EQE_{max} of 11.8% while a sky-blue emissive device with CIE coordinates of (0.17, 0.25) based on ***i*-2CzdOXD4CF$_3$Ph** was obtained with a higher EQE_{max} of 12.3%. The OLEDs employing the present TADF emitters all show higher EQE_{max} than their corresponding 1,2-isomers that we previously reported. This work and its contrast to our previous report reveals the importance of regiochemistry of donors and acceptors in the performance of deep blue OLEDs.

ASSOCIATED CONTENT

The Supporting Information is available free of charge on the ACS Publication website at DOI:

Complete experimental protocol; NMR spectra (Figure S1-S19); HPLC trace (Figure S20-S23); thermal characterization (Figure S24-S26); supplementary photophysical data (S27-S32); supplementary calculations (Figure S33-S34) and coordinates; angle-dependent PL measurements (Figure S35). CIF files for **2CzIPN**, ***i*-2CzdOXDMe**, ***i*-2CzdOXDPh** and ***i*-2CzdOXD4MeOPh** with CCDC 1918802-1918805.

ACKNOWLEDGEMENT

We are grateful to the EPSRC for financial support (grants EP/P010482/1, EP/J01771X, EP/J00916 and EP/R035164/1). We gratefully acknowledge funding through the EPSRC NSF-CBET lead agency agreement (EP/R010595/1, 1706207) and a Leverhulme Trust Research Grant (RPG-2017-231). We thank the EPSRC UK National Mass Spectrometry Facility at Swansea University for analytical services. Z.L. and W. L. thank the China Scholarship Council (grant numbers 201703780004 and 201708060003).

REFERENCES

(1.) White, M. S., et al., Ultrathin, Highly Flexible and Stretchable Pleds. *Nat. Photon.* **2013**, *7*, 811-816.
(2.) Sasabe, H.; Kido, J., Development of High Performance Oleds for General Lighting. *J. Mater. Chem. C* **2013**, *1*, 1699-1707.
(3.) Xu, R. P.; Li, Y. Q.; Tang, J. X., Recent Advances in Flexible Organic Light-Emitting Diodes. *J. Mater. Chem. C* **2016**, *4*, 9116-9142.
(4.) Lee, S. M.; Kwon, J. H.; Kwon, S.; Choi, K. C., A Review of Flexible Oleds toward Highly Durable Unusual Displays. *IEEE Transactions on Electron Devices* **2017**, *64*, 1922-1931.
(5.) Luo, D.; Chen, Q.; Liu, B.; Qiu, Y., Emergence of Flexible White Organic Light-Emitting Diodes. *Polymers* **2019**, *11*, 384.
(6.) Jeon, S. K.; Lee, H. L.; Yook, K. S.; Lee, J. Y., Recent Progress of the Lifetime of Organic Light-Emitting Diodes Based on Thermally Activated Delayed Fluorescent Material. *Adv. Mater.* **2019**, 1803524.

(7.) Liu, Y. F.; Feng, J.; Bi, Y. G.; Yin, D.; Sun, H. B., Recent Developments in Flexible Organic Light-Emitting Devices. *Adv. Mater. Technol.* **2019**, *4*, 1800371.
(8.) Smith, L. H.; Wasey, J. A. E.; Barnes, W. L., Light Outcoupling Efficiency of Top-Emitting Organic Light-Emitting Diodes. *Appl. Phys. Lett.* **2004**, *84*, 2986-2988.
(9.) Baldo, M. A.; O'Brien, D. F.; You, Y.; Shoustikov, A.; Sibley, S.; Thompson, M. E.; Forrest, S. R., Highly Efficient Phosphorescent Emission from Organic Electroluminescent Devices. *Nature* **1998**, *395*, 151-154.
(10.) Shi, S.; Jung, M. C.; Coburn, C.; Tadle, A.; Sylvinson, M. R. D.; Djurovich, P. I.; Forrest, S. R.; Thompson, M. E., Highly Efficient Photo- and Electroluminescence from Two-Coordinate Cu(I) Complexes Featuring Nonconventional N-Heterocyclic Carbenes. *J. Am. Chem. Soc.* **2019**, *141*, 3576-3588.
(11.) Zou, Y.; Gong, S. L.; Xie, G. H.; Yang, C. L., Design Strategy for Solution-Processable Thermally Activated Delayed Fluorescence Emitters and Their Applications in Organic Light-Emitting Diodes. *Adv. Opt. Mater.* **2018**, *6*, 1800568.
(12.) Yang, X. L.; Xu, X. B.; Zhou, G. J., Recent Advances of the Emitters for High Performance Deep-Blue Organic Light-Emitting Diodes. *J. Mater. Chem. C* **2015**, *3*, 913-944.
(13.) Wei, Q.; Fei, N. N.; Islam, A.; Lei, T.; Hong, L.; Peng, R. X.; Fan, X.; Chen, L.; Gao, P. Q.; Ge, Z. Y., Small-Molecule Emitters with High Quantum Efficiency: Mechanisms, Structures, and Applications in Oled Devices. *Adv. Opt. Mater.* **2018**, *6*, 1800512.
(14.) Bui, T.-T.; Goubard, F.; Ibrahim-Ouali, M.; Gigmes, D.; Dumur, F., Thermally Activated Delayed Fluorescence Emitters for Deep Blue Organic Light Emitting Diodes: A Review of Recent Advances. *Appl. Sci.* **2018**, *8*, 494.
(15.) Im, Y.; Kim, M.; Cho, Y. J.; Seo, J. A.; Yook, K. S.; Lee, J. Y., Molecular Design Strategy of Organic Thermally Activated Delayed Fluorescence Emitters. *Chem. Mater.* **2017**, *29*, 1946-1963.
(16.) Duan, C. B.; Li, J.; Han, C. M.; Ding, D. X.; Yang, H.; Wei, Y.; Xu, H., Multi-Dipolar Chromophores Featuring Phosphine Oxide as Joint Acceptor: A New Strategy toward High-Efficiency Blue Thermally Activated Delayed Fluorescence Dyes. *Chem. Mater.* **2016**, *28*, 5667-5679.
(17.) Liang, Q. Q.; Han, C. M.; Duan, C. B.; Xu, H., Blue Thermally Activated Delayed Fluorescence-Emitting Phosphine Oxide Hosts for Ultrasimple and Highly Efficient White Organic Light-Emitting Diodes. *Adv. Opt. Mater.* **2018**, *6*, 1800020.
(18.) Li, C.; Duan, C.; Han, C.; Xu, H., Secondary Acceptor Optimization for Full-Exciton Radiation: Toward Sky-Blue Thermally Activated Delayed Fluorescence Diodes with External Quantum Efficiency of Approximately 30. *Adv. Mater.* **2018**, *30*, 1804228.
(19.) Ye, J.; Chen, Z.; Fung, M.-K.; Zheng, C.; Ou, X.; Zhang, X.; Yuan, Y.; Lee, C.-S., Carbazole/Sulfone Hybrid D-Π-a-Structured Bipolar Fluorophores for High-Efficiency Blue-Violet Electroluminescence. *Chem. Mater.* **2013**, *25*, 2630-2637.
(20.) Zhang, Q. S.; Li, B.; Huang, S. P.; Nomura, H.; Tanaka, H.; Adachi, C., Efficient Blue Organic Light-Emitting Diodes Employing Thermally Activated Delayed Fluorescence. *Nat Photon.* **2014**, *8*, 326-332.
(21.) Fan, C.; Duan, C.; Han, C.; Han, B.; Xu, H., Dibenzothiophene Sulfone-Based Phosphine Oxide Electron Transporters with Unique Asymmetry for High-Efficiency Blue Thermally Activated Delayed Fluorescence Diodes. *ACS Appl. Mater. Interfaces* **2016**, *8*, 27383-27393.
(22.) Jurgensen, N.; Kretzschrnar, A.; Hofle, S.; Freudenberg, J.; Bunz, U. H. F.; Hernandez-Sosa, G., Sulfone-Based Deep Blue Thermally Activated Delayed Fluorescence Emitters: Solution-

Processed Organic Light-Emitting Diodes with High Efficiency and Brightness. *Chem. Mater.* **2017**, *29*, 9154-9161.
(23.) Li, J.; Zhang, R.; Wang, Z. Q.; Zhao, B.; Xie, J. J.; Zhang, F.; Wang, H.; Guo, K. P., Zig-Zag Acridine/Sulfone Derivative with Aggregation-Induced Emission and Enhanced Thermally Activated Delayed Fluorescence in Amorphous Phase for Highly Efficient Nondoped Blue Organic Light-Emitting Diodes. *Adv. Opt. Mater.* **2018**, *6*, 1701256.
(24.) Komatsu, R.; Ohsawa, T.; Sasabe, H.; Nakao, K.; Hayasaka, Y.; Kido, J., Manipulating the Electronic Excited State Energies of Pyrimidine-Based Thermally Activated Delayed Fluorescence Emitters to Realize Efficient Deep-Blue Emission. *ACS Appl. Mater. Interfaces* **2017**, *9*, 4742-4749.
(25.) Park, I. S.; Lee, J.; Yasud, T., High-Performance Blue Organic Light-Emitting Diodes with 20% External Electroluminescence Quantum Efficiency Based on Pyrimidine-Containing Thermally Activated Delayed Fluorescence Emitters. *J. Mater. Chem. C* **2016**, *4*, 7911-7916.
(26.) Park, I. S.; Komiyama, H.; Yasuda, T., Pyrimidine-Based Twisted Donor-Acceptor Delayed Fluorescence Molecules: A New Universal Platform for Highly Efficient Blue Electroluminescence. *Chem. Sci.* **2017**, *8*, 953-960.
(27.) Nakao, K.; Sasabe, H.; Komatsu, R.; Hayasaka, Y.; Ohsawa, T.; Kido, J., Significant Enhancement of Blue Oled Performances through Molecular Engineering of Pyrimidine-Based Emitter. *Adv. Opt. Mater.* **2017**, *5*, 1600843.
(28.) Wu, K.; Zhang, T.; Zhan, L.; Zhong, C.; Gong, S.; Jiang, N.; Lu, Z. H.; Yang, C., Optimizing Optoelectronic Properties of Pyrimidine-Based Tadf Emitters by Changing the Substituent for Organic Light-Emitting Diodes with External Quantum Efficiency Close to 25 % and Slow Efficiency Roll-Off. *Chem. Eur. J.* **2016**, *22*, 10860-10866.
(29.) Kim, M.; Jeon, S. K.; Hwang, S. H.; Lee, J. Y., Stable Blue Thermally Activated Delayed Fluorescent Organic Light-Emitting Diodes with Three Times Longer Lifetime Than Phosphorescent Organic Light-Emitting Diodes. *Adv. Mater.* **2015**, *27*, 2515-2520.
(30.) Lee, D. R.; Kim, M.; Jeon, S. K.; Hwang, S. H.; Lee, C. W.; Lee, J. Y., Design Strategy for 25% External Quantum Efficiency in Green and Blue Thermally Activated Delayed Fluorescent Devices. *Adv. Mater.* **2015**, *27*, 5861-5867.
(31.) Lin, T. A., et al., Sky-Blue Organic Light Emitting Diode with 37% External Quantum Efficiency Using Thermally Activated Delayed Fluorescence from Spiroacridine-Triazine Hybrid. *Adv. Mater.* **2016**, *28*, 6976-6983.
(32.) Lee, J.; Shizu, K.; Tanaka, H.; Nomura, H.; Yasuda, T.; Adachi, C., Oxadiazole- and Triazole-Based Highly-Efficient Thermally Activated Delayed Fluorescence Emitters for Organic Light-Emitting Diodes. *J. Mater. Chem. C* **2013**, *1*, 4599-4604.
(33.) Zhang, D.; Cao, X. D.; Wu, Q. J.; Zhang, M. C.; Sun, N.; Zhang, X. P.; Tao, Y. T., Purely Organic Materials for Extremely Simple All-Tadf White Oleds: A New Carbazole/Oxadiazole Hybrid Material as a Dual-Role Non-Doped Light Blue Emitter and Highly Efficient Orange Host. *J. Mater. Chem. C* **2018**, *6*, 3675-3682.
(34.) Cooper, M. W.; Zhang, X. Q.; Zhang, Y. D.; Jeon, S. O.; Lee, H.; Kim, S.; Fuentes-Hernandez, C.; Barlow, S.; Kippelen, B.; Marder, S. R., Effect of the Number and Substitution Pattern of Carbazole Donors on the Singlet and Triplet State Energies in a Series of Carbazole-Oxadiazole Derivatives Exhibiting Thermally Activated Delayed Fluorescence. *Chem. Mater.* **2018**, *30*, 6389-6399.
(35.) Chung, C. L.; Chen, H. C.; Yang, Y. S.; Tung, W. Y.; Chen, J. W.; Chen, W. C.; Wu, C. G.; Wong, K. T., S,N-Heteroacene-Based Copolymers for Highly Efficient Organic Field Effect

Transistors and Organic Solar Cells: Critical Impact of Aromatic Subunits in the Ladder Pi-System. *ACS Appl Mater Interfaces* **2018**, *10*, 6471-6483.
(36.) Zhang, X.; Cooper, M. W.; Zhang, Y.; Fuentes-Hernandez, C.; Barlow, S.; Marder, S. R.; Kippelen, B., Host-Free Yellow-Green Organic Light-Emitting Diodes with External Quantum Efficiency over 20% Based on a Compound Exhibiting Thermally Activated Delayed Fluorescence. *ACS Appl. Mater. Interfaces* **2019**, *11*, 12693-12698.
(37.) Uoyama, H.; Goushi, K.; Shizu, K.; Nomura, H.; Adachi, C., Highly Efficient Organic Light-Emitting Diodes from Delayed Fluorescence. *Nature* **2012**, *492*, 234-8.
(38.) Cho, Y. J.; Yook, K. S.; Lee, J. Y., Cool and Warm Hybrid White Organic Light-Emitting Diode with Blue Delayed Fluorescent Emitter Both as Blue Emitter and Triplet Host. *Sci. Rep.* **2015**, *5*, 7859.
(39.) Zhang, Q.; Li, J.; Shizu, K.; Huang, S.; Hirata, S.; Miyazaki, H.; Adachi, C., Design of Efficient Thermally Activated Delayed Fluorescence Materials for Pure Blue Organic Light Emitting Diodes. *J. Am. Chem. Soc.* **2012**, *134*, 14706-9.
(40.) Rajamalli, P.; Chen, D.; Li, W.; Samuel, I. D. W.; Cordes, D. B.; Slawin, A. M. Z.; Zysman-Colman, E., Enhanced Thermally Activated Delayed Fluorescence through Bridge Modification in Sulfone-Based Emitters Employed in Deep Blue Organic Light-Emitting Diodes. *J. Mater. Chem. C* **2019**, advance article.
(41.) Tamoto, N.; Adachi, C.; Nagai, K., Electroluminescence of 1,3,4-Oxadiazole and Triphenylamine-Containing Molecules as an Emitter in Organic Multilayer Light Emitting Diodes. *Chem. Mater.* **1997**, *9*, 1077-1085.
(42.) Huang, W.; Meng, H.; Yu, W. L.; Gao, J.; Heeger, A. J., A New Blue Light-Emitting Polymer Containing Substituted Thiophene and an Arylene-1,3,4-Oxadiazole Moiety. *Adv. Mater.* **1998**, *10*, 593-596.
(43.) Schulz, B.; Bruma, M.; Brehmer, L., Aromatic Poly(1,3,4-Oxadiazole)S as Advanced Materials. *Adv. Mater.* **1997**, *9*, 601-613.
(44.) Tao, Y.; Yang, C.; Qin, J., Organic Host Materials for Phosphorescent Organic Light-Emitting Diodes. *Chem. Soc. Rev.* **2011**, *40*, 2943-70.
(45.) Tan, Y.; Rui, B.; Li, J.; Zhao, Z.; Liu, Z.; Bian, Z.; Huang, C., Blue Thermally Activated Delayed Fluorescence Emitters Based on a Constructing Strategy with Diversed Donors and Oxadiazole Acceptor and Their Efficient Electroluminescent Devices. *Opt. Mater.* **2019**, *94*, 103-112.
(46.) Adamo, C.; Barone, V., Toward Reliable Density Functional Methods without Adjustable Parameters: The Pbe0 Model. *J. Chem. Phys.* **1999**, *110*, 6158-6170.
(47.) Pople, J. A. B., J. S.; Seeger, R., Theoretical Models Incorporating Electron Correlation. *Int. J. Quant. Chem. Symp.* **1976**, 1-19.
(48.) Grimme, S., Density Functional Calculations with Configuration Interaction for the Excited States of Molecules. *Chem. Phys. Lett.* **1996**, *259*, 128-137.
(49.) Hirata, S. H.-G., M., Time-Dependent Density Functional Theory within the Tamm–Dancoff Approximation. *Chem. Phys. Lett.* **1999**, 291-299.
(50.) D.B.Romero, M. S., M. Leclerc, D. Ades, A. Siove, L. Zuppiroli, The Role of Carbazole in Organic Light-Emitting Devices. *Synth. Met.* **1996**, 271-277.
(51.) Melhuish, W. H., Quantum Efficiencies of Fluorescence of Organic Substances: Effect of Solvent and Concentration of the Fluorescent Solute. *J. Phys. Chem.* **1961**, 229-235.

(52.) Cardona, C. M.; Li, W.; Kaifer, A. E.; Stockdale, D.; Bazan, G. C., Electrochemical Considerations for Determining Absolute Frontier Orbital Energy Levels of Conjugated Polymers for Solar Cell Applications. *Adv. Mater.* **2011**, *23*, 2367-2371.
(53.) Adachi, C., Third-Generation Organic Electroluminescence Materials. *Jpn. J. Appl. Phys.* **2014**, *53*, 060101.
(54.) Jeong, S. H.; Lee, J. Y., Dibenzothiophene Derivatives as Host Materials for High Efficiency in Deep Blue Phosphorescent Organic Light Emitting Diodes. *J. Mater. Chem. C* **2011**, *21*, 14604-14609.
(55.) Watanabe, Y.; Sasabe, H.; Kido, J., Review of Molecular Engineering for Horizontal Molecular Orientation in Organic Light-Emitting Devices. *Bull. Chem. Soc. Jpn.* **2019**, *92*, 716-728.
(56.) Kim, K. H.; Kim, J. J., Origin and Control of Orientation of Phosphorescent and Tadf Dyes for High-Efficiency Oleds. *Adv. Mater.* **2018**, *30*, 1705600.
(57.) Schmidt, T. D.; Lampe, T.; Sylvinson M. R, D.; Djurovich, P. I.; Thompson, M. E.; Brütting, W., Emitter Orientation as a Key Parameter in Organic Light-Emitting Diodes. *Phys. Rev. Appl.* **2017**, *8*, 037001.
(58.) Graf, A.; Liehm, P.; Murawski, C.; Hofmann, S.; Leo, K.; Gather, M. C., Correlating the Transition Dipole Moment Orientation of Phosphorescent Emitter Molecules in Oleds with Basic Material Properties. *J. Mater. Chem. C* **2014**, *2*, 10298-10304.

TOC

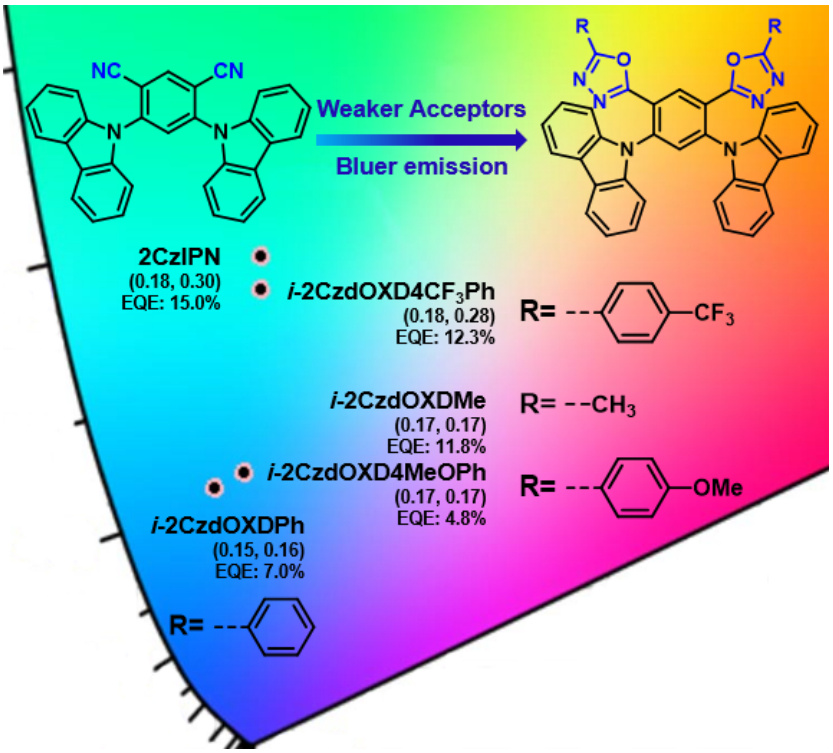
NC
CN
N
N
Weaker Acceptors
Bluer emission
R
R
O
N
N
O
N
N
N
N
2CzIPN
(0.18, 0.30)
EQE: 15.0%
i-2CzdOXD4CF3Ph
(0.18, 0.28)
EQE: 12.3%
R= CF3
i-2CzdOXDMe
(0.17, 0.17)
EQE: 11.8%
R= CH3
i-2CzdOXD4MeOPh
(0.17, 0.17)
EQE: 4.8%
R= OMe
i-2CzdOXDPh
(0.15, 0.16)
EQE: 7.0%
R=